Predicting Microstructure-Creep Resistance Correlation in High Temperature Alloy over Multiple Time Scales

Prof. Vikas Tomar (PI) & Hongsuk Lee

School of Aeronautics and Astronautics, Purdue University

Prof. Jian Luo (co-PI), Naixie Zhou & Yuanyao Zhang

University of California, San Diego & Clemson University

➢Thermodynamic Modelling

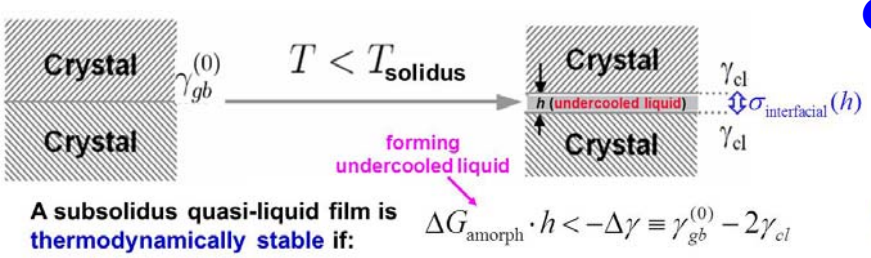

Define & quantify:

$$\lambda \equiv \frac{-\Delta\gamma}{\Delta G_{amorph}}$$

λ represents the thermodynamic tendency for grain boundaries (GBs) to disorder

Reference:

Luo, *Journal of the American Ceramic Society* 95: 2358 (2012)

Computed GB λ-Diagrams to Represent Levels of GB Disorder

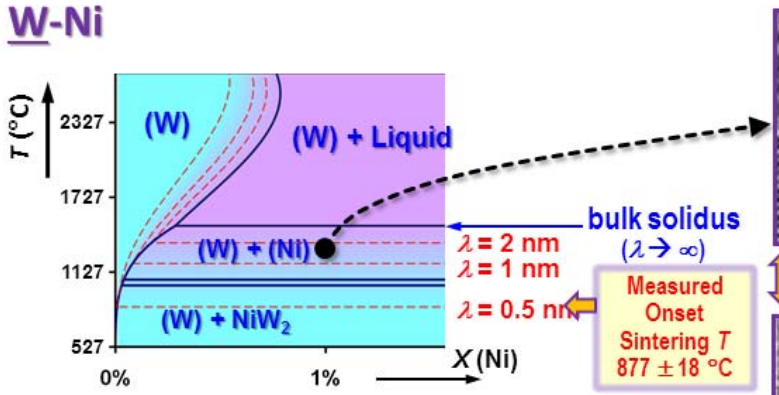

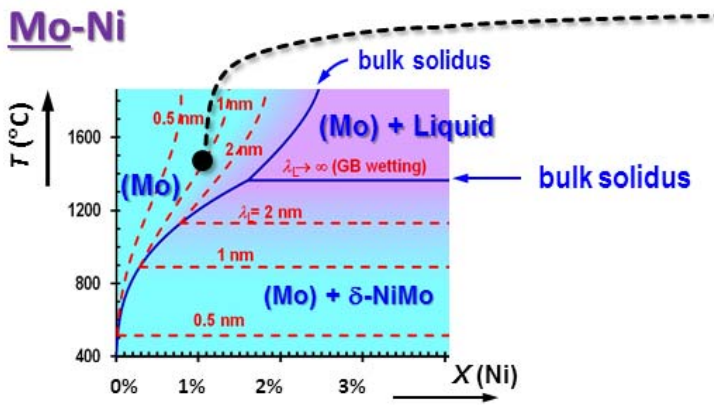

Validations…

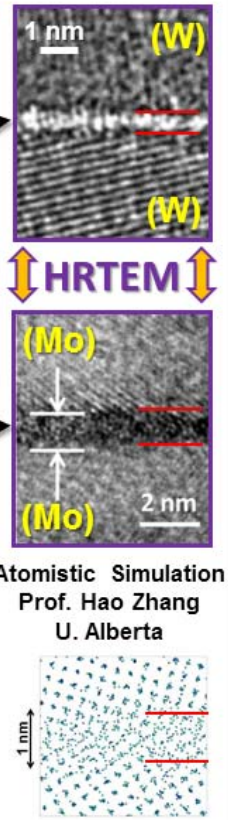

➢To Predict (Coble) Creep?

Extending Bulk CalPhaD Methods to GBs (Prior Successful Studies)

Computed GB Diagram (Level of GB Disorder)

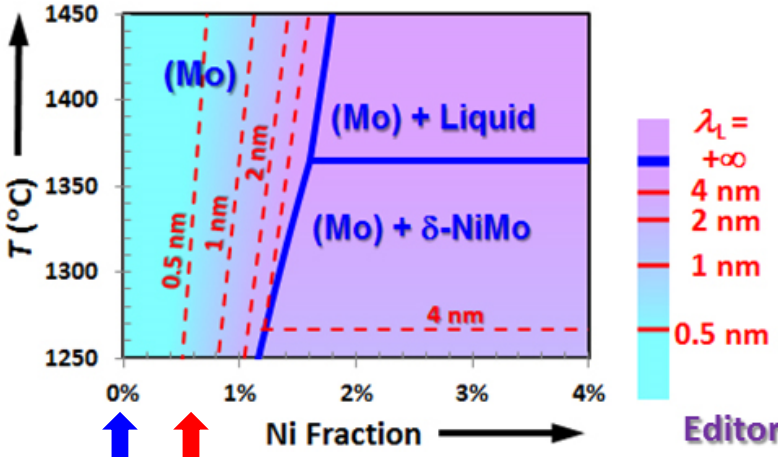

Model Experimental Comparison

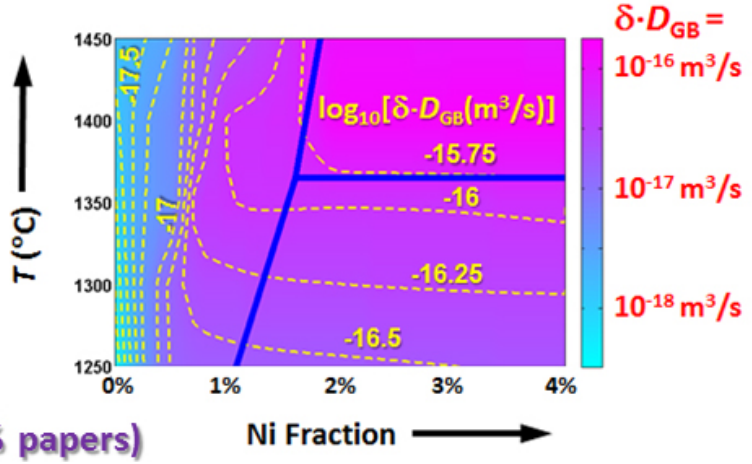

Shi & Luo
Phys. Rev. B 2011
Editors' Suggestion (4%-8% papers)

Example of Predictability:
A counterintuitive prediction of D_{GB} ↓ as T ↑ was verified!

Shi & Luo
PRL 2010

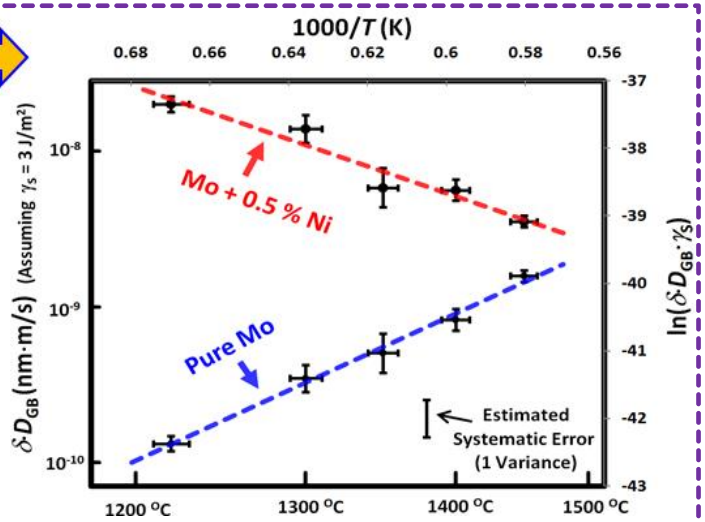

Experimentally-Measured GB Diffusivities

To Predict Coble Creep?

➢Preparing Nanocrystalline Ni and Ni-W Specimens for Mechanical Test

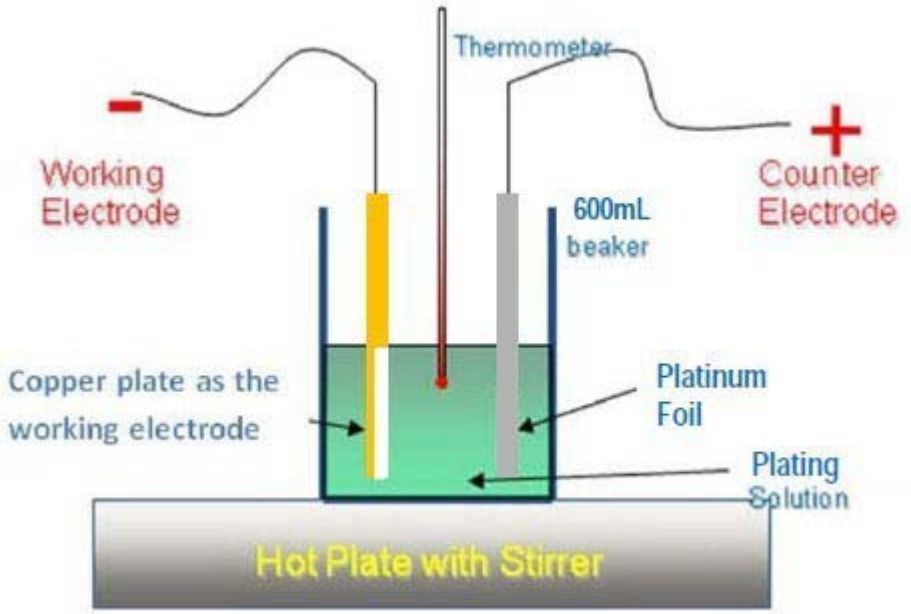

Temperature: 65 °C

Deposition time: 30 min to 2h

Chemicals	Weight(g/L)
$NiSO_4.6H_2O$	300
$NiCl_2.6H_2O$	45
H_3BO_3	45
Saccharine	5
Sodium Lauryl Sulfonate ($CH_3(CH_2)_{11}OSO_2Na$)	0.25

Current		Time (ms)	Peak (A/cm^2)
Forwards	On	5	0.4
	off	15	

El-Sherik, *et* al., J of Materials Science 30, 5743 (1995)

➢Free-Standing Nanocrystalline Ni Specimens

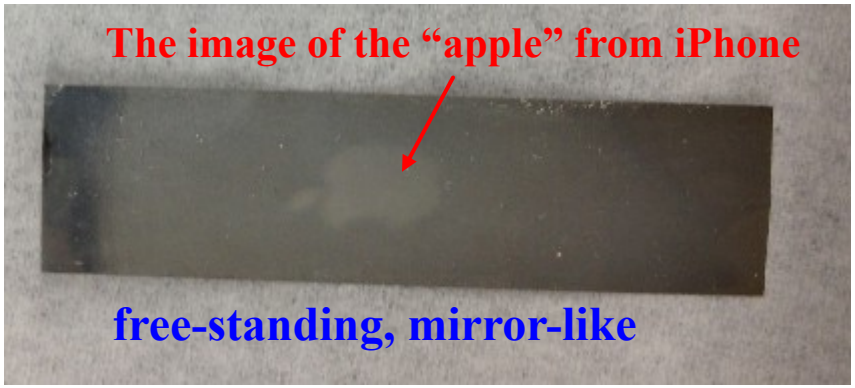

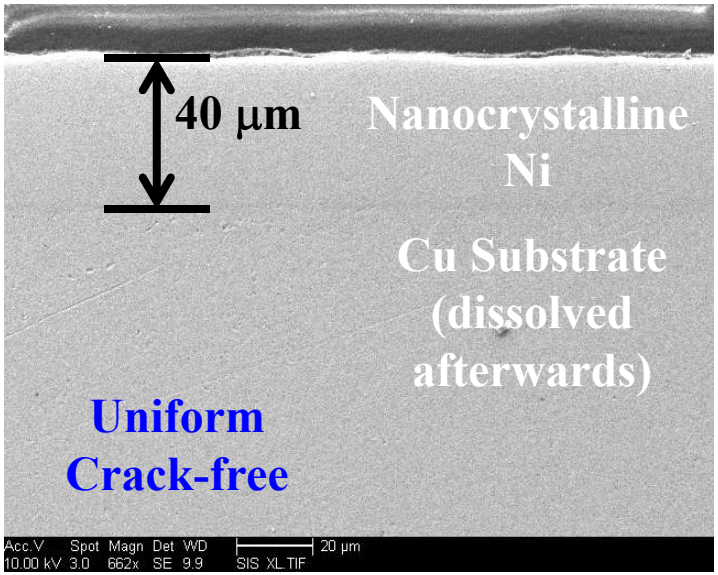

Grain Size (from the Scherrer equation) is ~18 nm.

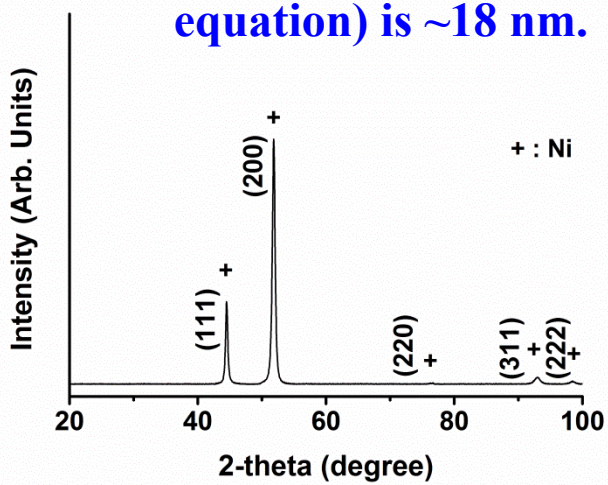

Current effort to make thicker specimens to fit the requirements for Purdue's *in-situ*, high-T, mechanical tests.

Nanocrystalline Ni-W alloy specimens (up to ~50 wt. % W) specimens were also successfully made.

➢Sintered Nanocrystalline W Alloys

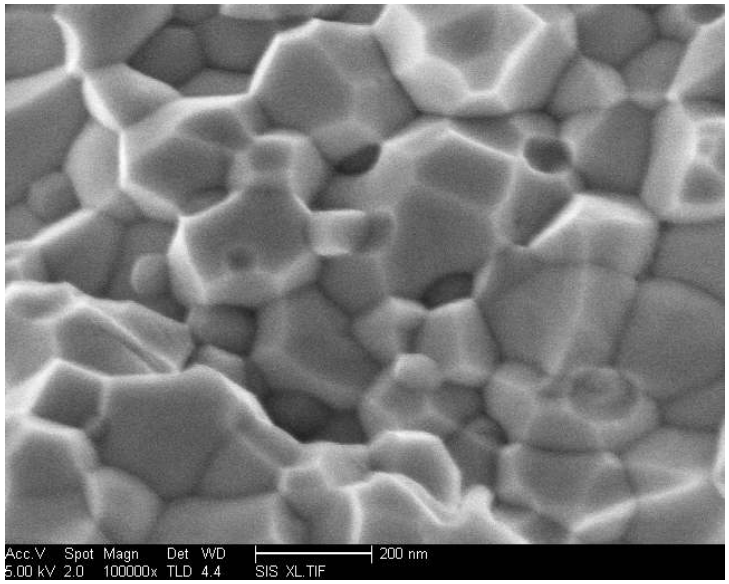

Grain Size:
~150 nm

~96% of the
Theoretical Density

➢Quantum mechanical calculation of GB Strength

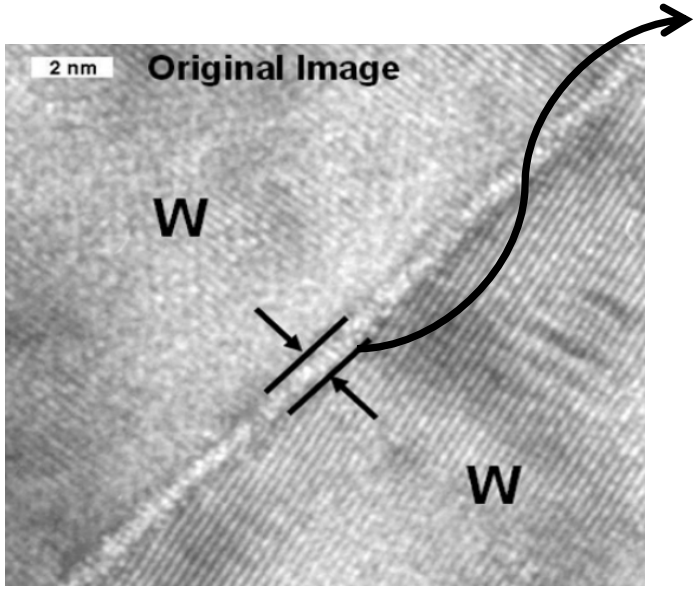

[Vivek K. Gupta and et al., 2007]

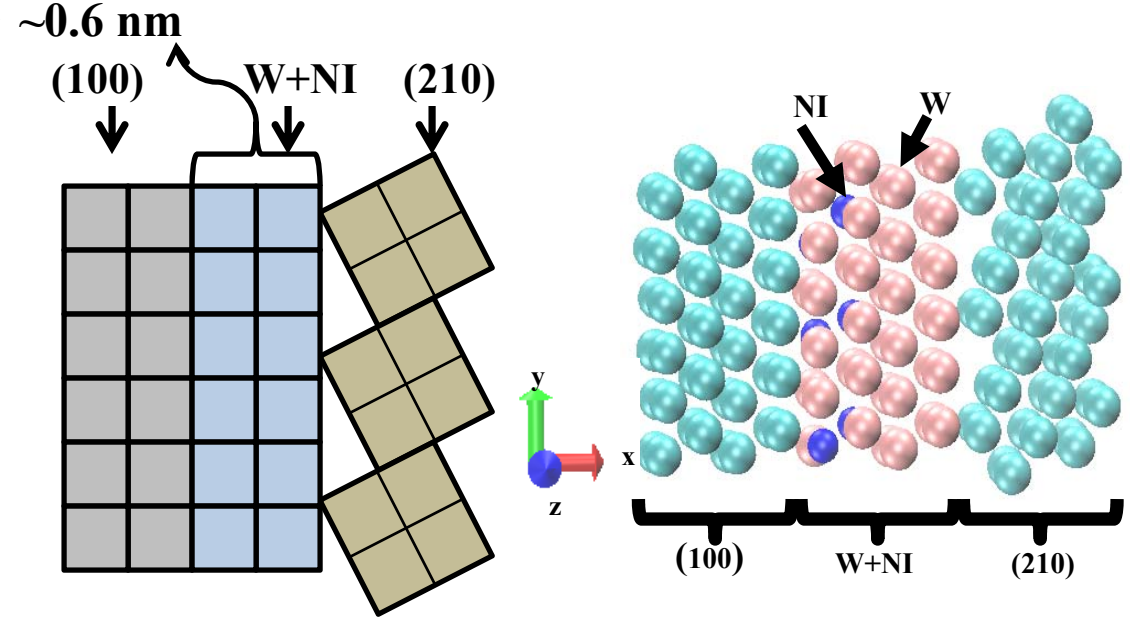

- ❖ time step: 5 a.u. , total 2000 steps — Becquart and et al., 2006
- ❖ cutoff energy for wavefunction : 350 eV — Nose and Shuichi, 1984
- ❖ Nose-Hoover thermostat : 300K, 400K, 500K, 600K — Hoover and William, 1985
- ❖ electronic fake mass for CPMD : 400 a.u. — Perdew and et al., 1996 Vanderbilt and David, 1990
- ❖ number of k-points for integration over Brillouin zone : 32x32x32 — Monkhorst and Pack., 1996

➢Stress – strain relation

(1) Unsaturated Ni - W

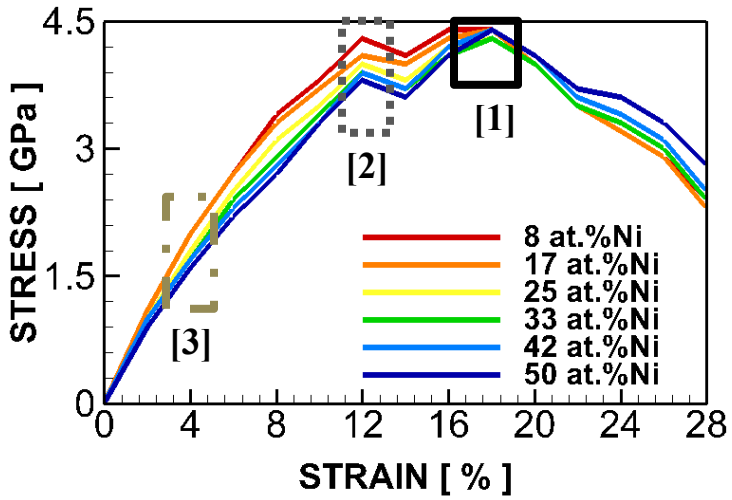

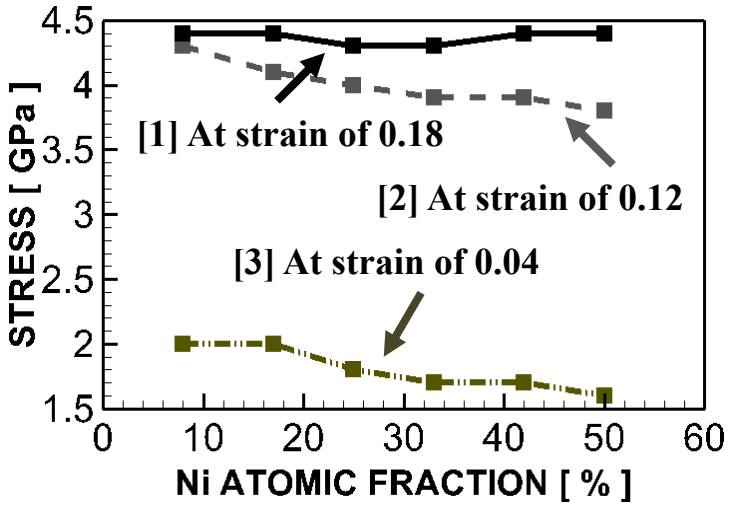

Yield strength: at strain 4%,

First peak: at strain 12%

Yield strength and first peak's values have dependent on the Ni volume fraction.

Second peak: at strain 18%

The second peak's values are not depend on the Ni volume fraction.

Ultimate tensile strength : strain of 12~18%

The maximum tensile strength is not affected by Ni volume fraction for the unsaturated W-Ni.

(2) Saturated Ni - W

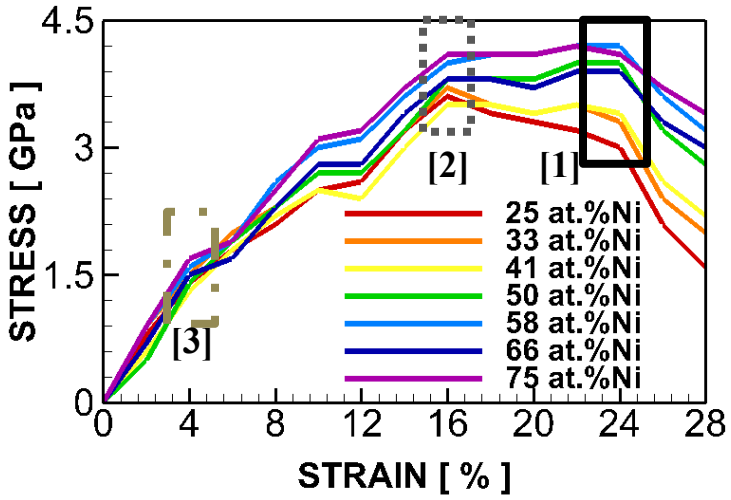

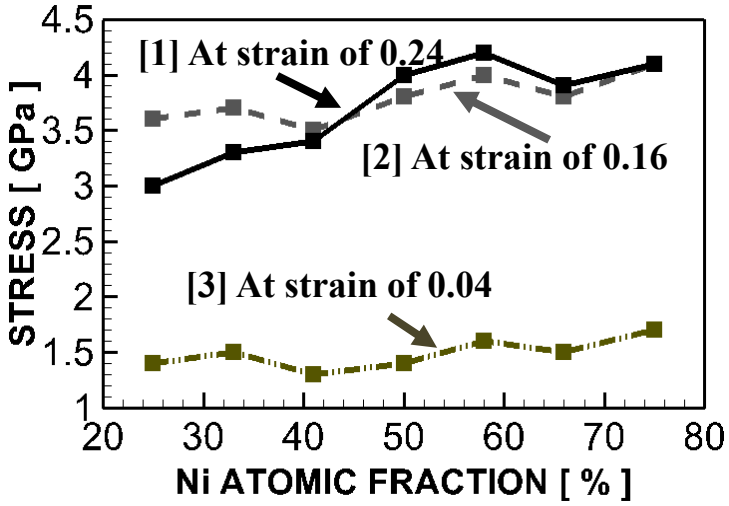

Yield strength: at strain 4%,
First peak: at strain 16%
Yield strength and first peak's values have dependent on the Ni volume fraction.
Second peak: at strain 24%
The second peak's values have the largest dependence on the Ni volume fraction.
Ultimate tensile strength : strain of 16~24%
The maximum tensile strength is not affected by Ni volume fraction for the saturated W-Ni.

➢Electron density distribution

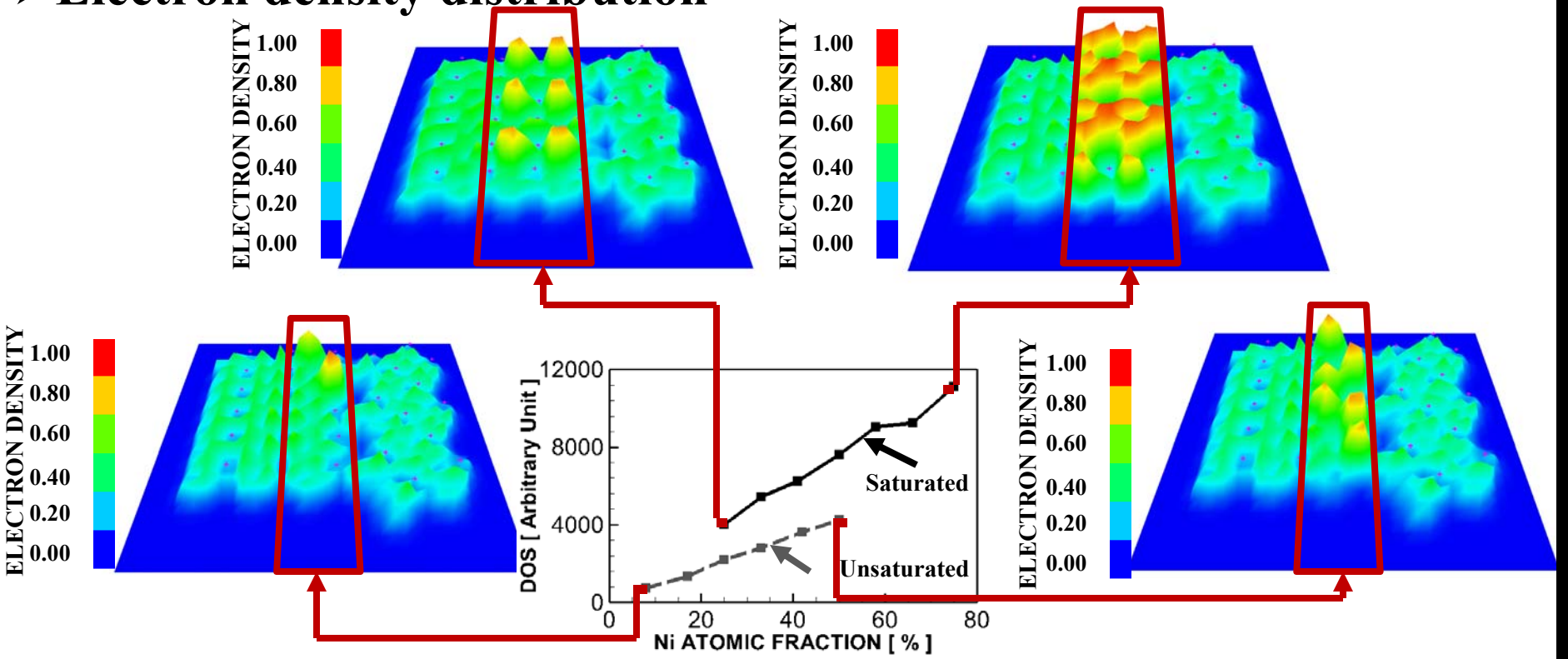

➢Electron density of states (f-orbital)

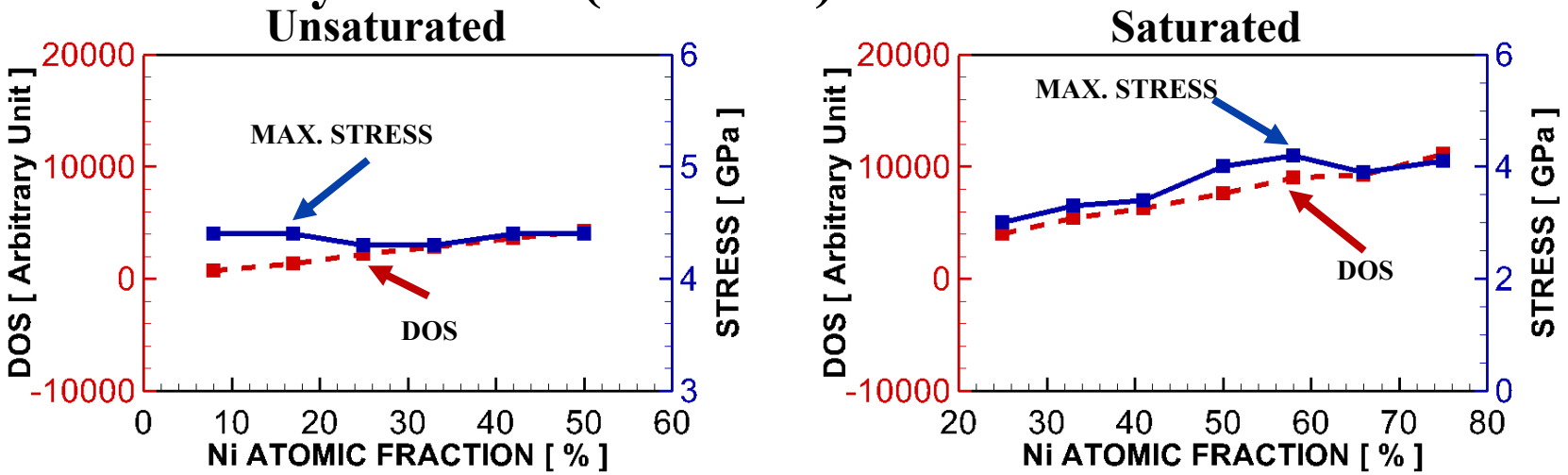

➢Phonon dispersion

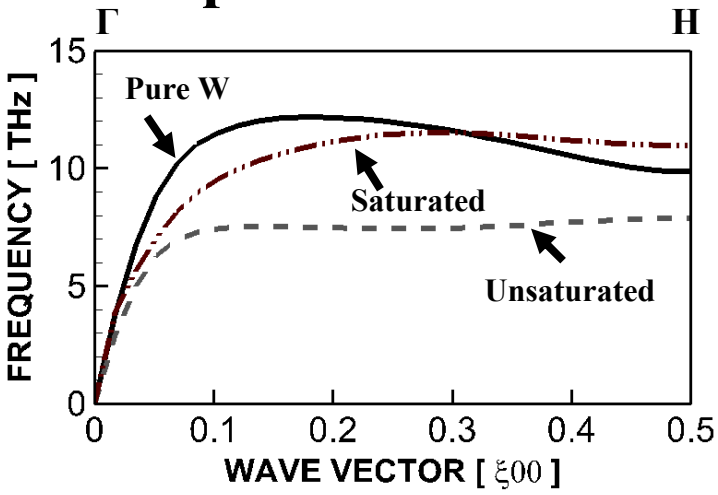

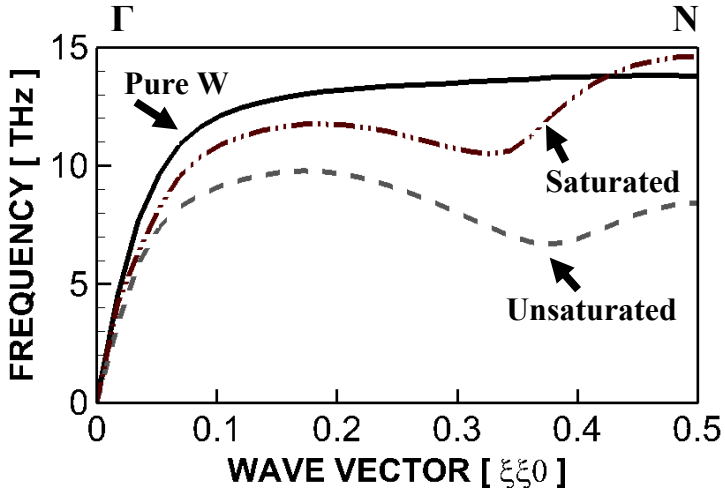

➢Prediction of peak tensile strength

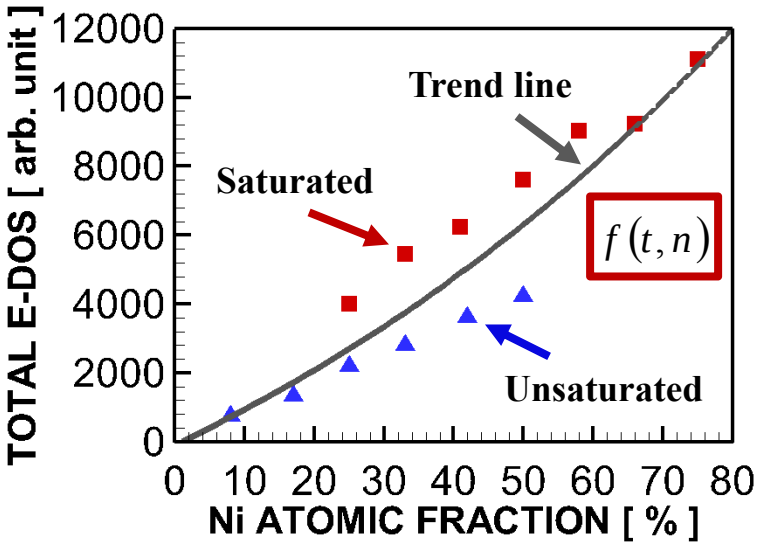

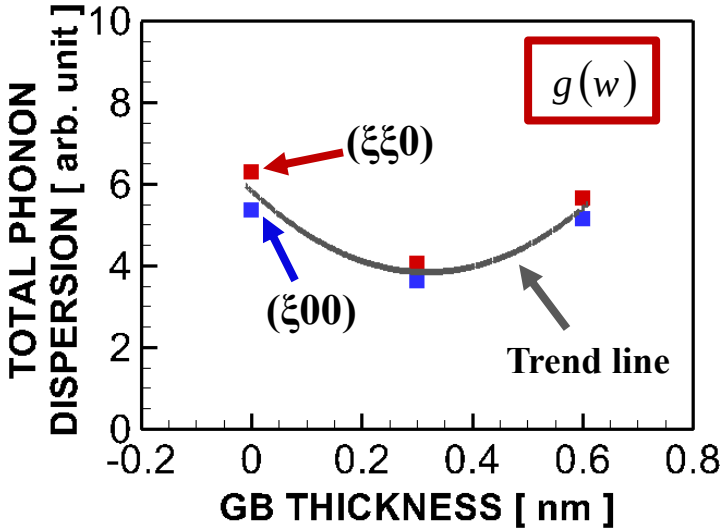

$$\frac{T_{max}}{T_{ideal}} = \cdot \frac{CE}{CD} \cdot \frac{1}{\Phi} \cdot f(t,n) \cdot g(w)$$

T_{max} : Maximum tensile strength of W-Ni alloy
T_{ideal} : Idealistic maximum tensile strength of W
Φ : Surface energy of W
CE : Atomic level cohesive energy of W

How does this prediction apply to continuum scale fracture?

➢Continuum scale model

(1) Nano-scale model

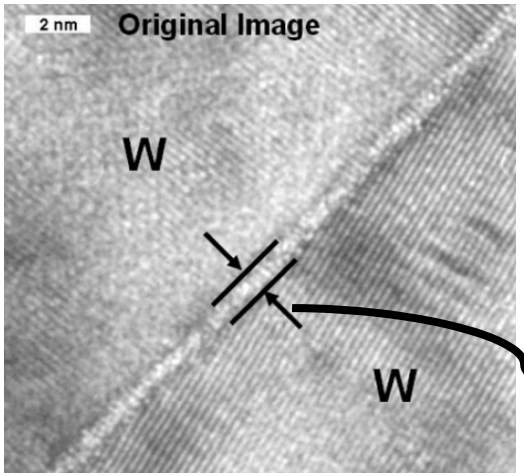

[V. Gupta et al, 2007]

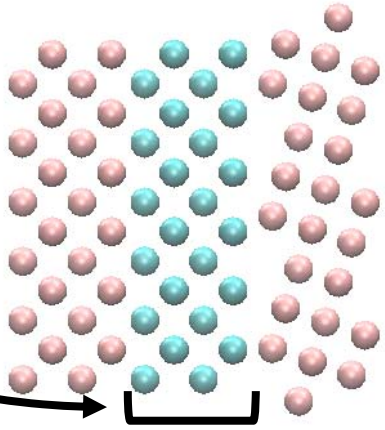

0.6nm

2nm

Bi-granular model

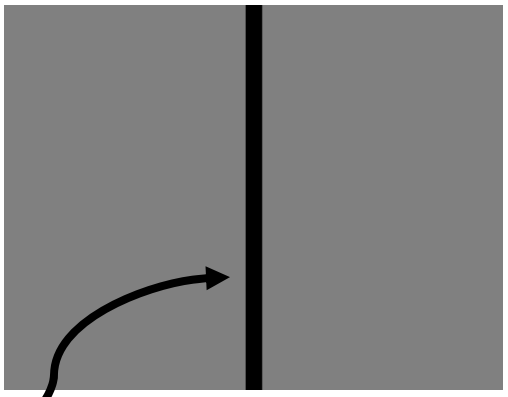

60nm

60nm

(2) Micro-scale model

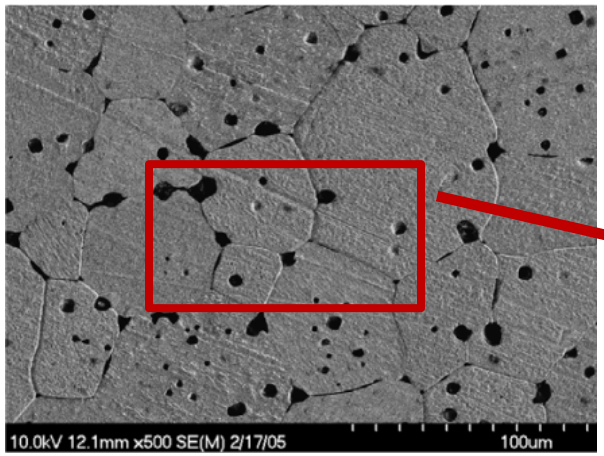

[V. Gupta et al, 2007]

Polycrystalline model

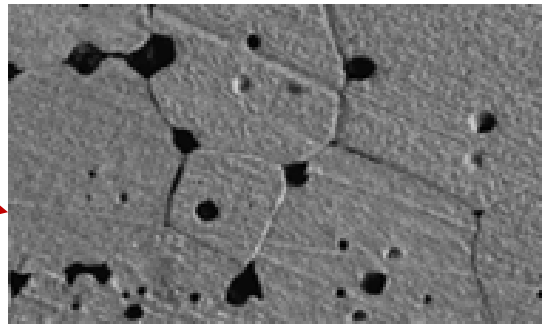

t = 10 μm

80 μm

135 μm

➢Material model of grains and GBs

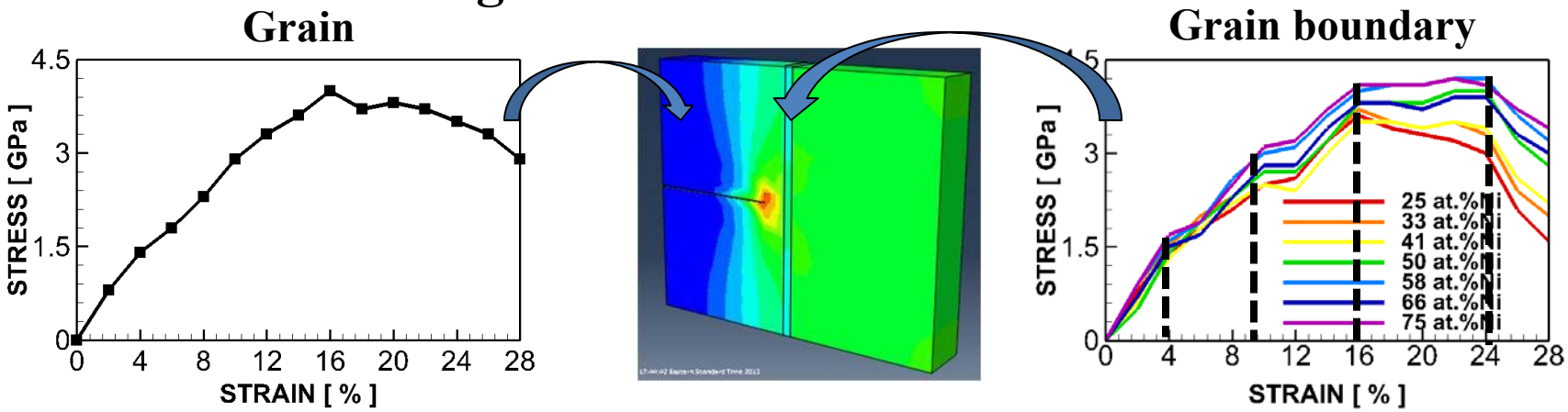

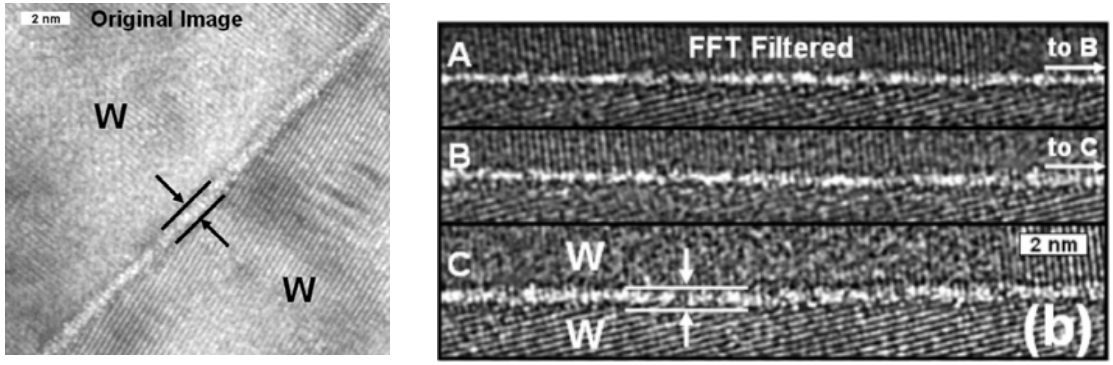

[V. Gupta et al, 2007]

Crack propagation of GB

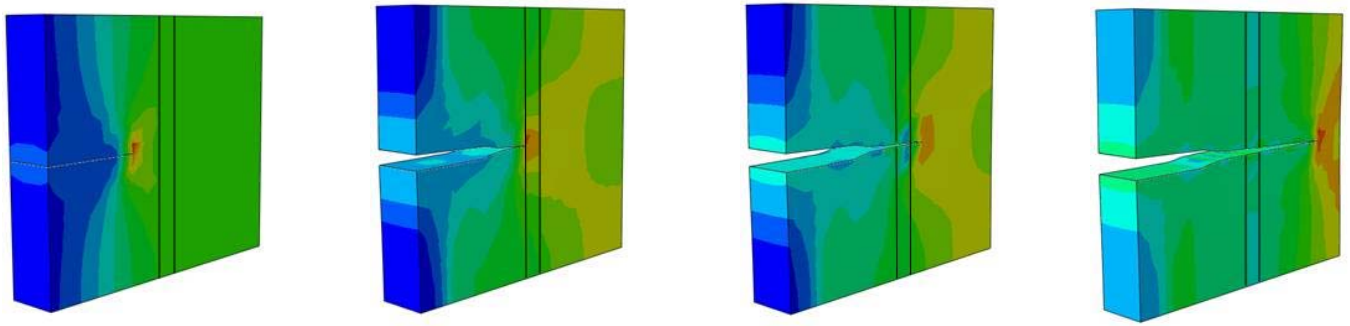

Time-step increment	4.5E-5	0.013	0.015	0.018

➢Fracture toughness analysis

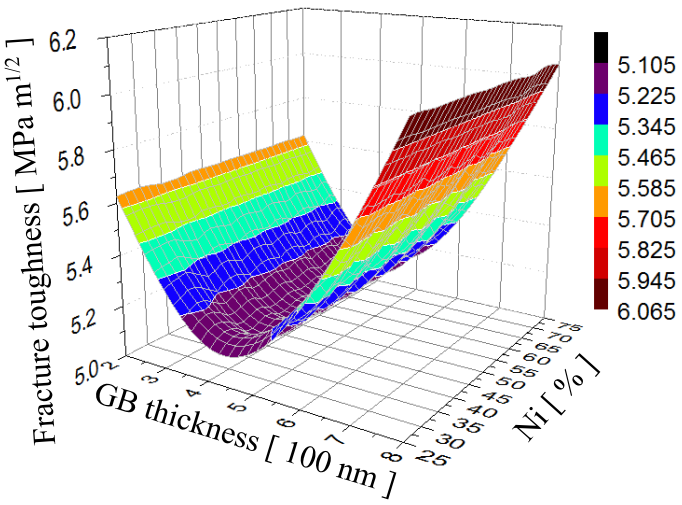

Fracture toughness in crack initiation

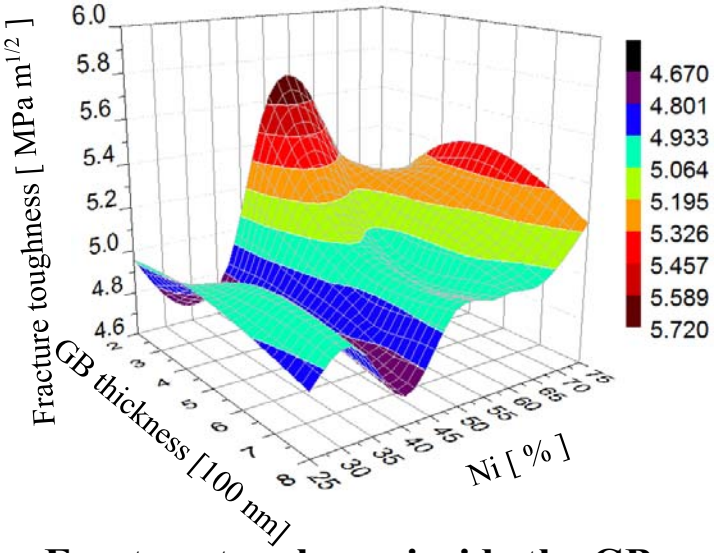

Fracture toughness inside the GB

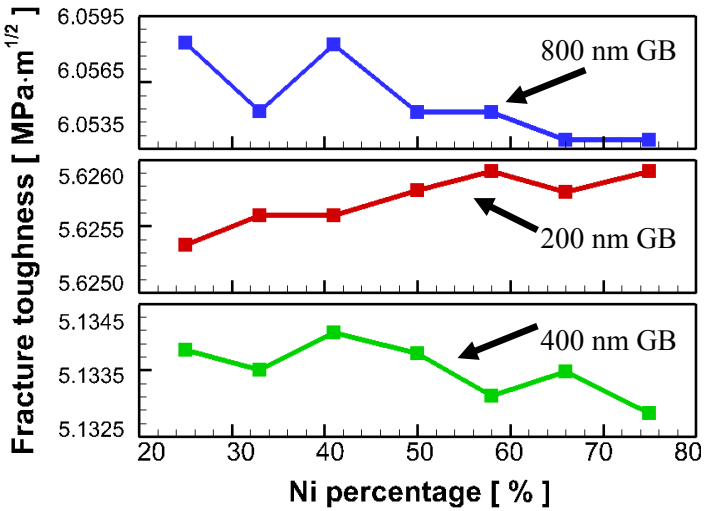

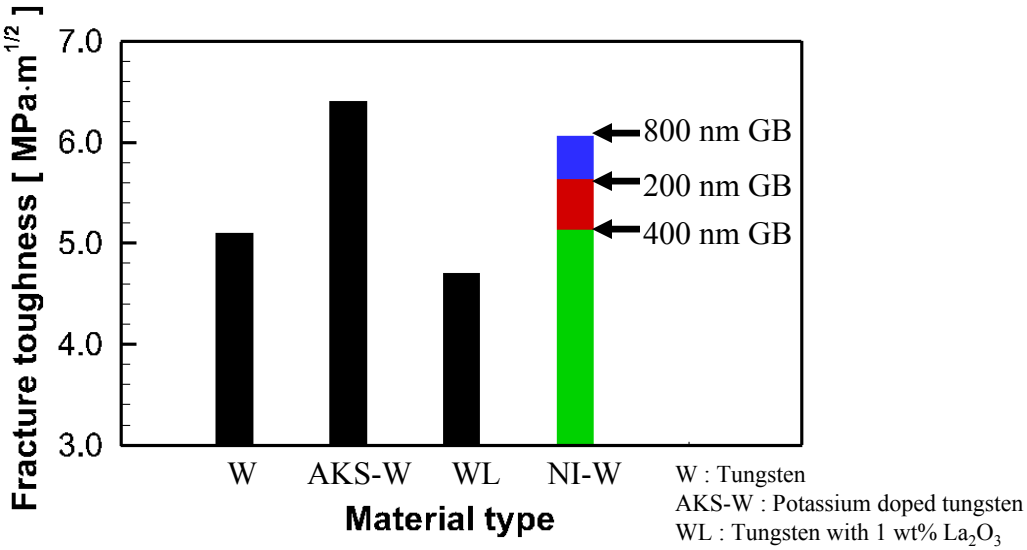

W : Tungsten
AKS-W : Potassium doped tungsten
WL : Tungsten with 1 wt% La_2O_3

[B. Gludovatz and et al., 2010]

➢Brittleness index of GBs

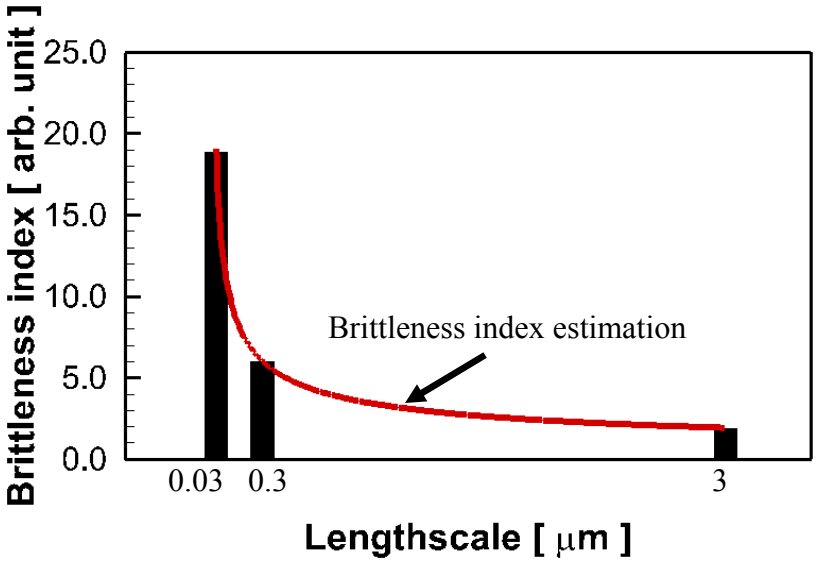

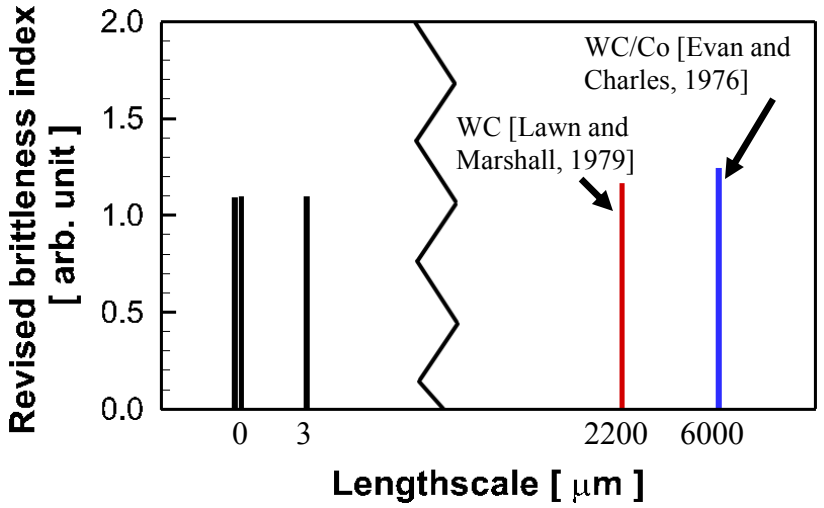

Effect of length-scale : $B = 3.3L^{-1/2}$

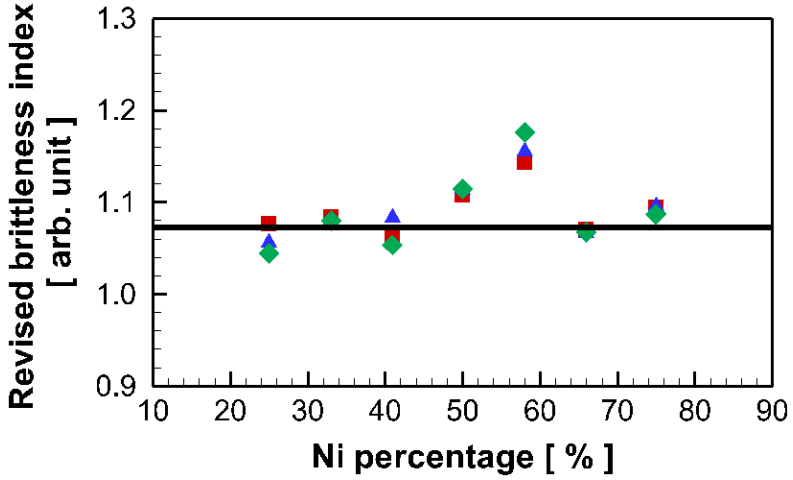

$$B^* = \frac{H}{K_c} \cdot \frac{1}{\alpha} \sqrt{L}$$

$\alpha = 3.3$ for W-Ni

Nomenclature

B*	brittleness index (no unit)
L	lengthscale (μm)
T	max. tensile strength (fracture strength)
H	hardness (GPa)
Kc	fracture toughness (MPa m^1/2)
t	GB thickness (μm)
p	Ni fraction (no unit)

➢ **Measurement of GB embrittlement has been obtained using the revised brittleness index.**

➢ **This provides an absolute range of qualitative measurement to describe the brittleness without considering the length scale limitations.**

➢Crack propagation in different angled GBs

θ = 90° θ = 80° θ = 70° θ = 60° θ = 50°

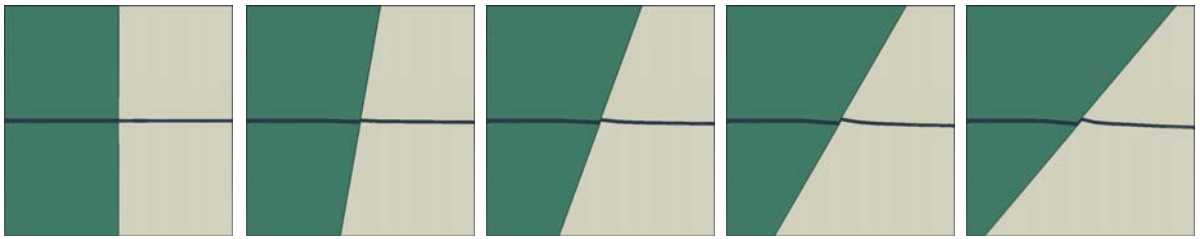

θ = 40° θ = 30° θ = 20° θ = 10°

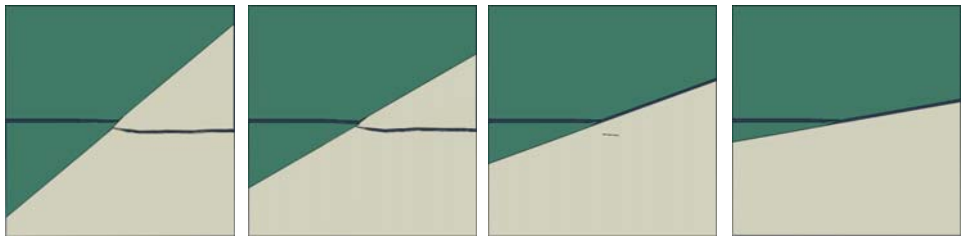

➢Inter-granular failure is represented as 1

➢Trans-granular failure is represented as -1

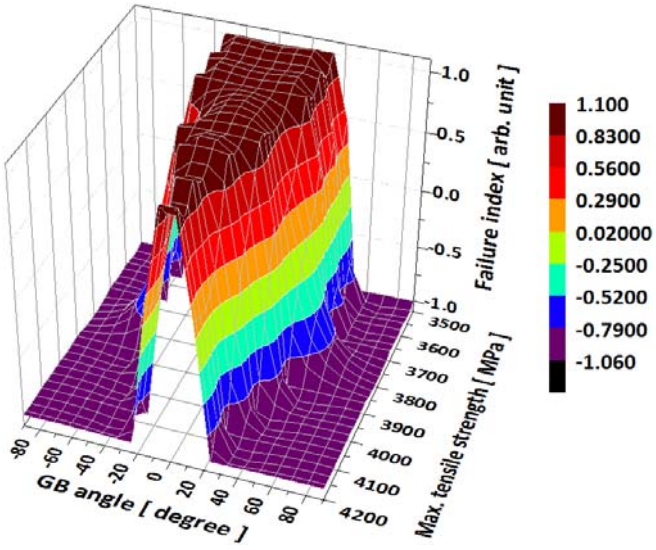

GB angle from -90 to 90 degree

❖**<u>Failure index</u>** : An index (between -1 and 1) to describe failure type, which can be either inter-granular failure or trans-granular failure.

$$FI = a + b\frac{T_{GB}}{T_{Grain}} + c\theta^2$$

a = 4.45
b = -4.2
c = -0.00024

Using the heavi-side function

$$H[FI] = \begin{cases} 1, & FI \geq 0 \\ -1, & FI < 0 \end{cases}$$

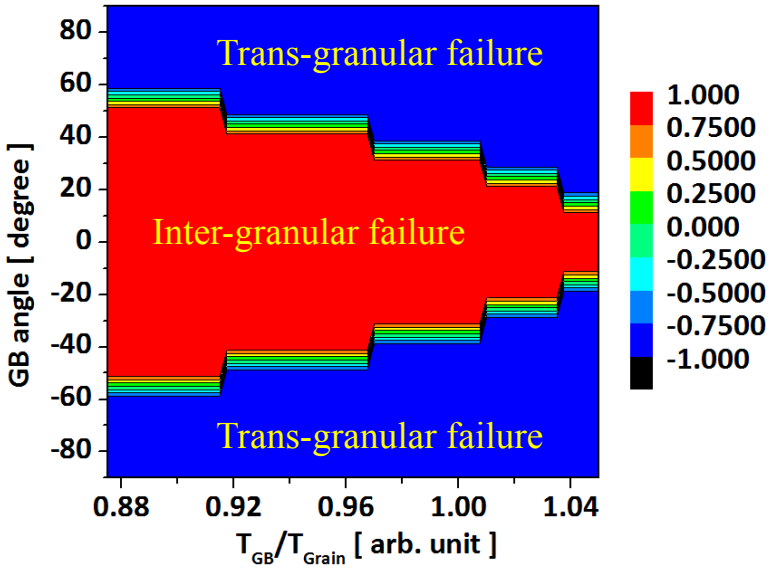

➢Validation and Conclusion

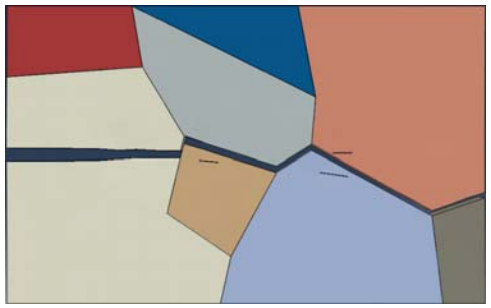
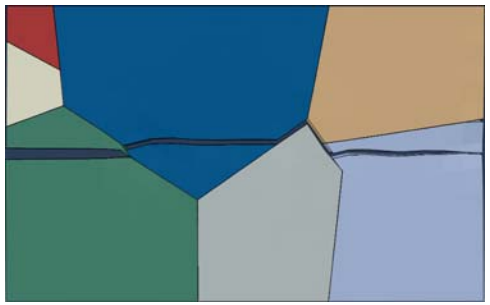
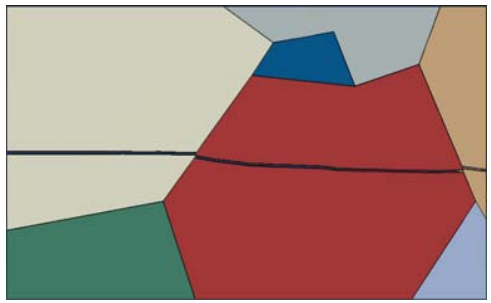

➢Perfect inter-granular failure has occurred.
➢Contains crack path with maximum GB angle of 67°.
➢GB strength property can be predicted.

$$FI = a + b\frac{T_{GB}}{T_{Grain}} + c\theta^2$$

➢According to the failure index prediction, given microstructure has max. tensile strength ratio between GB and grain as $T_{GB} \le (0.803) \cdot T_{Grain}$.

✓For various failed morphologies of polycrystalline W-Ni, GB's strength property can be predicted using the derived failure type criteria.

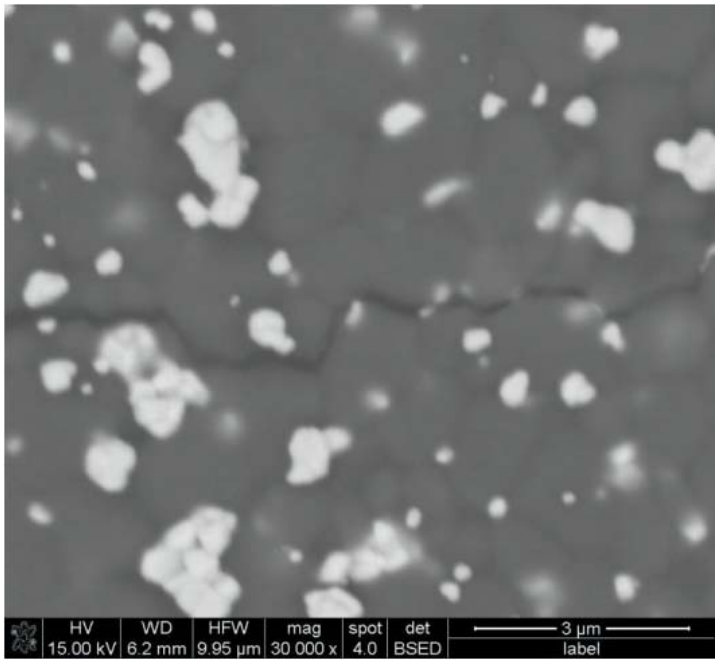

[Zbigniew Pedzich, 2012]

➢Acknowledgement

❖ **Support from DEO-NETL Grant DEFE0011291 is gratefully acknowledged.**

➢Publications

▪Gan, M. and Tomar, V. (2010). "Temperature dependent multiscale creep strength of a class of polymer derived Si-C-O ceramics." Acta Materialia (submitted).
▪Gupta, V. K., Yoon, D.-H., Meyer Iii, H. M. and Luo, J. (2007a). "Thin intergranular films and solid-state activated sintering in nickel-doped tungsten." Acta Materialia 55(9): 3131-3142.
▪Gupta, V. K., Yoon, D. H., Meyer, H. M. and Luo, J. (2007b). "Thin intergranular films and solid-state activated sintering in nickel-doped tungsten." Acta Materialia 55(9): 3131-3142.
▪Lee, H. and Tomar, V. (2014). "Understanding the influence of grain boundary thickness variation on the mechanical strength of a nickel-doped tungsten grain boundary." International Journal of Plasticity 53: 135-147.
▪Luo, J. and Shi, X. M. (2008). "Grain boundary disordering in binary alloys." Applied Physics Letters 92(10).
▪Shi, X. and Luo, J. (2011). "Developing grain boundary diagrams as a materials science tool: A case study of nickel-doped molybdenum." Physical Review B 84(1): 014105.
▪Shi, X. M. and Luo, J. (2009). "Grain boundary wetting and prewetting in Ni-doped Mo." Applied Physics Letters 94(25).
▪Tomar, V. (2007). Multiscale simulation of dynamic fracture in polycrystalline SiC-Si 3 N 4 using a molecularly motivated cohesive finite element method. 48th AIAA/ASME/ASCE/AHS/ASC Structures, Structural Dynamics, and Materials Conference (April 23-26, 2007) Honolulu, Hawaii, Paper No. AIAA-2007-2345.
▪Tomar, V. (2008a). "Analyses of the role of grain boundaries in mesoscale dynamic fracture resistance of SiC-Si 3 N 4 intergranular nanocomposites." Eng. Fract. Mech. 75: 4501-4512.
▪Tomar, V. (2008b). "Analyses of the role of the second phase SiC particles in microstructure dependent fracture resistance variation of SiC-Si 3 N 4 nanocomposites." Modelling Simul. Mater. Sci. Eng. 16: 035001.
▪Tomar, V. (2008c). "Modeling of dynamic fracture and damage in 2-Dimensional trabecular bone microstructures using the cohesive finite element method." J. Biomech. Engg. 130(2): 021021.
▪Tomar, V., Zhai, J. and Zhou, M. (2004). "Bounds for element size in a variable stiffness cohesive finite element model." Int. J. Num. Meth. Engg. 61: 1894-1920.
▪Tomar, V. and Zhou, M. (2006). "Tension-compression strength asymmetry of nanocrystalline α -Fe 2 O 3 +fcc-Al ceramic-metal composites." Appl. Phys. Lett. 88: 233107 (233101-233103).
▪Tomar, V. and Zhou, M. (2007). "Analyses of tensile deformation of nanocrystalline α -Fe 2 O 3 +fcc-Al composites using classical molecular dynamics." J. Mech. Phys. Solids 55 1053-1085.
▪Zhai, J., Tomar, V. and Zhou, M. (2004). "Micromechanical modeling of dynamic fracture using the cohesive finite element method." J. Engg. Mat. Tech. 126: 179-191.